ROYAL SOCIETY OF CHEMISTRY

PAPER

Check for updates

Discovery of novel azole derivatives with benzanilide-containing hydrophobic side chains for the treatment of drug-resistant fungal infections†

Hao Jia, [ID] [a] Sha-sha Gong,[a] Yong-xin Zhang,[a] Ying-xia Xie*[ab] and Naying Chu*[a]

As fungal resistance to existing antifungal drugs continues to rise, there is an urgent need for new drugs with anti-resistance activity. In this study, a series of newly designed and synthesized benzanilide-containing azoles exhibited promising antifungal activity against fluconazole-sensitive *Candida albicans*. Importantly, the newly synthesized compounds also displayed potent activity against azole-resistant strains, surpassing the performance of the positive control fluconazole. This suggests that these compounds may have the potential to combat drug-resistant fungal infections. Subsequent studies on the antifungal mechanisms revealed that the compound can inhibit fungal CYP51, thereby blocking ergosterol biosynthesis. Morphological observations of fungal cells further confirmed CYP51 as the target of action. Resistance mechanisms elucidated that these compounds can inhibit biofilm formation and the expression of resistance-related genes ERG11 and efflux pump gene CDR1, thereby reversing resistance. Meanwhile, the most potent compound **A11** demonstrated the ability to stimulate reactive oxygen species, thereby exhibiting potent fungicidal activity. Furthermore, the compound **A11** also showed good stability in liver microsomes and plasma metabolism. Cytotoxicity studies demonstrated low toxicity of the compounds against MRC-5 cells, indicating their potential safety for therapeutic use. *In vivo* experimental results indicated that the representative compound **A11** significantly inhibited fungal infections caused by resistant strains. Molecular docking studies further supported the efficacy of compound **A11**, showing its ability to bind to *Candida albicans* CYP51. These findings highlight the promising antifungal activity and minimal cytotoxicity of the benzanilide-containing azoles, making them potential candidates for the treatment of drug-resistant fungal infections.

1. Introduction

With the increasing number of human immunodeficiency disease patients and the use of anti-tumor chemotherapy drugs, the incidence of fungal infection has shown an increasing trend year by year and the invasive infection has become one of the important causes of clinical death.[1–4] At present, antifungal drugs are mainly composed of polyenes (*e.g.*, amphotericin B), echinococcus (*e.g.*, caspofungin), allylamines (*e.g.*, terbinafine) and azole drugs (Fig. 1).[5] Azole drugs such as imidazole (*e.g.*, miconazole, MCZ), triazole (*e.g.*, fluconazole, FLC) and tetrazoles (*e.g.*, oteseconazole) are widely used in clinic because of their excellent therapeutic effect. However, the overuse of azole drugs has led to the emergence of drug-resistant strains, making the treatment of fungal infections more difficult.[6] It is

aDepartment of Pharmacy, The First People's Hospital of Shangqiu, Suiyang District, 292 Kaixuan Road, Shangqiu 476000, China. E-mail: chunaying@sina.com; yingxia725@126.com

bSchool of Pharmaceutical Sciences, Zhengzhou University, Zhengzhou 450001, China
† Electronic supplementary information (ESI) available. See DOI: https://doi.org/10.1039/d5ra00461f

urgent to accelerate the development of new antifungal drugs to deal with the increasing number of drug-resistant fungi. Considering the clinical therapeutic advantages of azole drugs, we still focused on the modification of azole drugs in this study.

2. Results and discussion

2.1. The design of benzamide-containing azoles compounds

The azole class of antifungal drugs inhibits fungal lanosterol 14-α-demethylase (CYP51) activity through competitive bind to the enzyme's heme cofactor.[7,8] Therefore, it is necessary to analyze the structural characteristics of CYP51 inhibitors. As is well known, the CYP51 protein, in addition to the heme ring, contains two hydrophobic channels in its protein cavity, namely hydrophobic channel I and II as shown in the Fig. 2.[9,10] In general, we can use the nitrogen-containing heterocyclic to bind to the heme, and the two hydrophobic segments to bind to the two hydrophobic channels. Particularly, hydrophobic channel II is relatively narrow, making it difficult for larger fragments to penetrate into this channel.[11] The benzanilide fragment, being relatively flat, has the potential to extend into this channel. Therefore, in this study, the benzanilide fragment was chosen
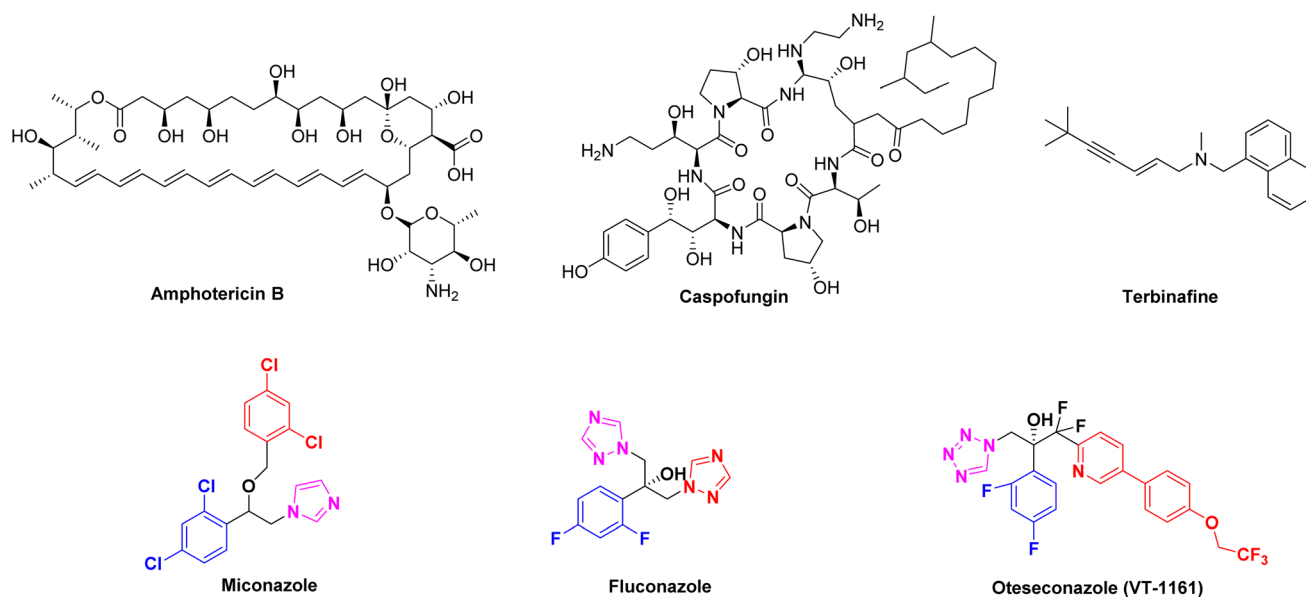
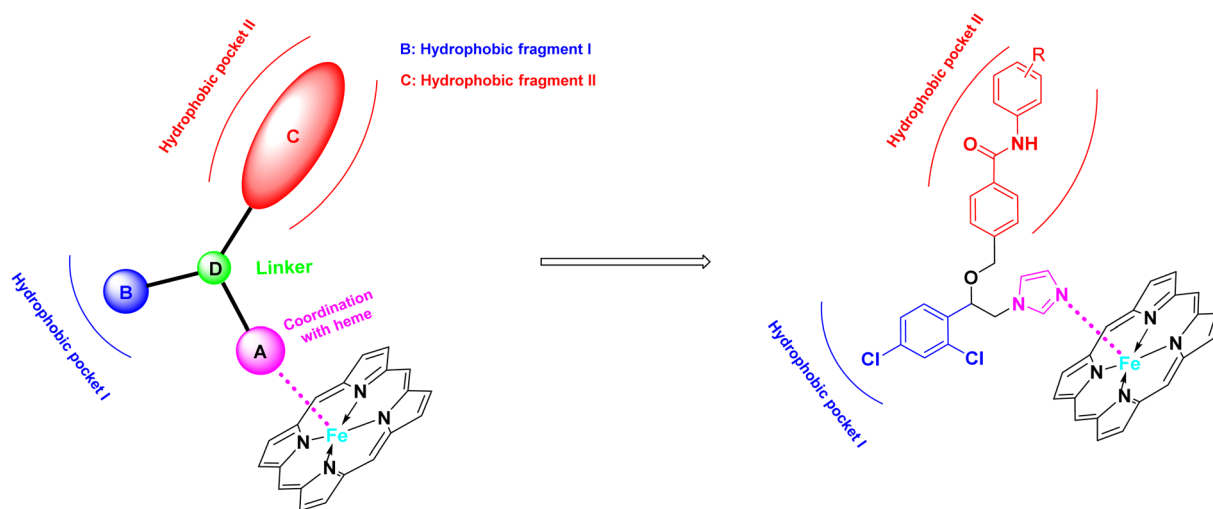Fig. 1   The chemical structures of clinical antifungal drugs.

Fig. 2   Design strategies for target compounds.

as hydrophobic fragment II for the first time, with the expectation that it would extend into the narrow hydrophobic channel II, thereby enhancing antifungal activity (Fig. 2). Based on this design rationale, compounds **A01–A15** were synthesized and evaluated for their antifungal activity using microdilution methods. Further, the mechanism, cytotoxicity, metabolic stability and *in vivo* efficiency were studied.

2.2. Chemistry

The general synthetic routes of target compounds **A01–A15** were outlined in Scheme 1. Firstly, intermediate **3** were prepared from substituted α-bromoacetophenone **1** upon treatment with imidazole in the presence of triethylamine. Then, the carbonyl group of intermediate **3** was reduced to intermediate **4** using sodium borohydride. Compound **4** reacted with methyl 4-

(bromomethyl) benzoate to generate intermediate **5**. After hydrolysis of intermediate **5**, it was condensed with various substituted anilines to yield the final products **A01–A15**.

2.3. *In vitro* antifungal activity against fluconazole-sensitive *Candida albicans* strains

The antifungal activity of these compounds was assessed against five species of *C. alb* (5314), *C. par*, *C. gla*, *C. kru* and *C. neo*. The minimum inhibitory concentrations (MIC_{80}) were determined to quantify the degree of growth inhibition, with fluconazole and miconazole being used as positive controls for comparison. Interestingly, compounds **A01–A15** exhibited moderate to strong antifungal activity against all of the tested fungi. Moreover, there was a clear structure–activity relationship observed among these compounds, suggesting that
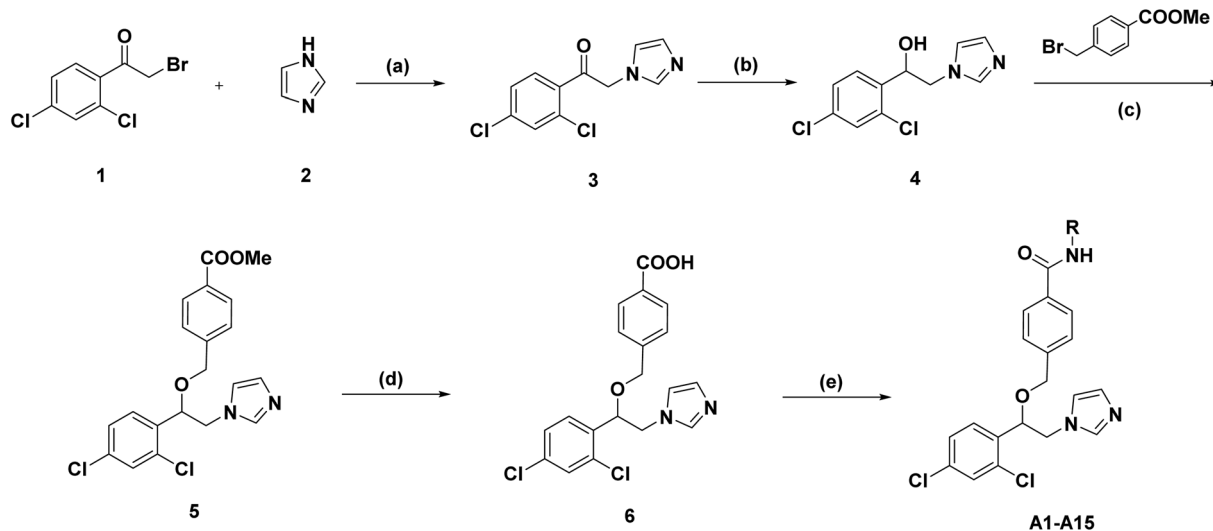
Scheme 1 Synthetic route of target compounds **A01–A15**. Reagents and conditions: (a) Et$_3$N, MeOH, 65 °C, 4 h, 90%; (b) NaBH$_4$, MeOH, 25 °C, 2 h, 80%. (c) NaH, tetrahydrofuran, 70 °C, 4 h, 65.5%; (d) KOH, MeOH, reflux, 1 h (without purification); (e) R-NH$_2$, DCM, DMAP, EDCI, 25 °C, 1 h.

specific structural features are responsible for their antifungal activity (Table 1). When R is substituted monocycle, compounds **A1–A11** exhibit good antifungal activity. The MIC$_{80}$ values of these compounds range from 0.03 to 0.5 µg mL^{-1}, which are superior to those of the positive control drug fluconazole. As analogs of miconazole, these compounds exhibited better inhibitory activity against both *C. alb* (5314) and *C. kru* compared to miconazole. In contrast, when R is substituted bicyclic, compounds **A12**, **A13** and **A14** exhibit decreased antifungal activity (MIC = 2–64 µg mL^{-1}). This could be due to the larger size of the bicyclic substituent, which may form unfavorable interactions in the narrow channel II. The antifungal activity significantly decreases when the R group contains a hydrogen bond donor, such as compounds **A15** (MIC = 32– >128 µg mL^{-1}). This may be because channel II is hydrophobic and cannot accommodate hydrogen bond donor groups within this hydrophobic channel.

2.4. Analysis of sterol composition in *C. albicans* (SC5314)

GC-MS was employed to investigate the antifungal mechanism of the target compounds by determining the changes in sterol content in fungal cell membrane.[12] Fluconazole was used as a positive control in this study. The model strain *C. alb* 5314 was incubated with the drugs for 24 hours to detect the alterations in sterol content. The results, presented in Fig. 3, demonstrate that fluconazole and compound **A11** effectively suppresses ergosterol biosynthesis in fungal cell membranes, leading to significant accumulations of obtusifoliol, lanosterol, and eburicol. These findings suggest that our compounds exert their antifungal activity by inhibiting the enzyme CYP51, involved in the biosynthesis of ergosterol.

2.5. Morphological observation of fungal cells

The GC-MS analysis experiment preliminarily proved that the target of our compounds is CYP51. It is well known that the

azole drugs inhibit the biosynthesis of ergosterol by inhibiting the activity of CYP51, thereby increasing the permeability of cell membranes and leading to fungal death. Therefore, the observation of cell membrane morphology can further directly prove that the target of our compound is CYP51. To complete this experiment, we chosen *C. alb* 5314 as the test strain and applied transmission electron microscopy (TEM) to observe the morphology changes of the fungal cell membrane after the drug was added. The experimental results were shown in Fig. 4. It can be observed that the fungal cells in the control group presented a regular and complete structure. After the addition of drugs or fluconazole, the cell membrane was damaged and the contents leak out into the surrounding area. That said, compound **A11** could indeed disrupt the structural integrity of the cells, ultimately resulting in the breakdown and death of the fungus. This result is consistent with the physiological function of CYP51, which further proves that the target of our compounds is CYP51.

2.6. *In vitro* antifungal activity against fluconazole-resistant *Candida albicans* strains

The widespread occurrence of fungal resistance exacerbates the difficulty of treatment of fungal infection.[13–15] For the new compounds, if they have anti-drug resistance activity, it will have further development value. Thus, we further determined the antifungal activity of all the target compounds against five fluconazole-resistant strains obtained from clinical isolation. Fluconazole was used as a reference drug in this study. As indicated in Table 2, all target compounds exhibited significant antifungal activity against the tested resistant strains. Among these compounds, **A11** also displayed the most potent effects with MIC$_{80}$ values of 0.125–2 µg mL^{-1} on the tested strains. In contrast, fluconazole was completely inactive. These findings suggest that compound **A11** has the ability to effectively overcome fluconazole resistance. Subsequently, we also conducted preliminary studies on the mechanisms of drug resistance.

Table 1 The antifungal activity of the target compounds A01–A15

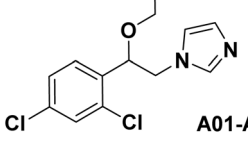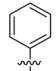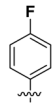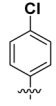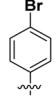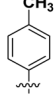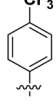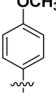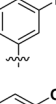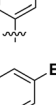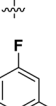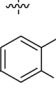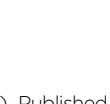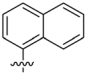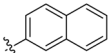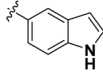| Compd	R	MIC$_{80}$/(μg mL^{-1})				
		C. alb (SC5314)	*C. par*	*C. gla*	*C. kru*	*C. neo*
A01	(phenyl)	0.125	0.125	0.25	0.25	0.25
A02	(4-F-phenyl)	0.125	0.125	0.25	0.06	0.5
A03	(4-Cl-phenyl)	0.125	0.25	0.125	0.125	0.06
A04	(4-Br-phenyl)	0.06	0.125	0.125	0.06	0.25
A05	(4-CH$_3$-phenyl)	0.03	0.06	0.06	0.125	0.25
A06	(4-CF$_3$-phenyl)	0.06	0.06	0.125	0.125	0.125
A07	(4-OCH$_3$-phenyl)	0.06	0.125	0.125	0.125	0.25
A08	(3-F-phenyl)	0.06	0.125	0.125	0.25	0.125
A09	(3-Cl-phenyl)	0.03	0.06	0.25	0.25	0.125
A10	(3-Br-phenyl)	0.25	0.125	0.125	0.06	0.125
A11	(2,4-diF-phenyl)	0.03	0.03	0.03	0.03	0.06
A12	(quinolinyl)	8	2	8	8	4

Table 1 (*Contd.*)

| Compd | R | MIC$_{80}$/(μg mL^{-1}) | | | | |
		C. alb (SC5314)	*C. par*	*C. gla*	*C. kru*	*C. neo*
A13		8	4	8	16	64
A14		32	32	64	32	32
A15		128	32	128	>128	128
Fluconazole		4	2	8	16	8
Miconazole		0.25	0.06	0.125	0.5	0.125

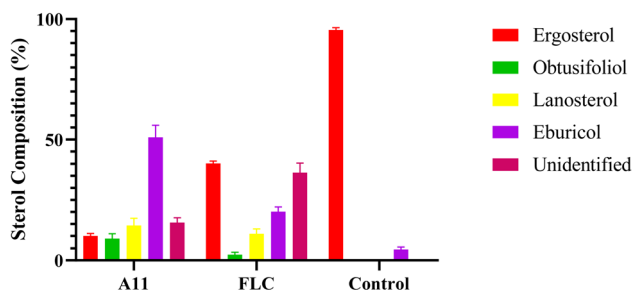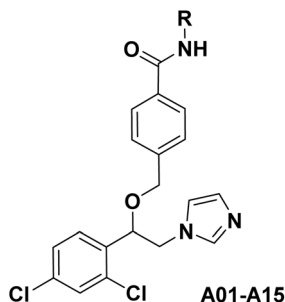**Fig. 3** Sterol composition analysis. **FLC** and **A11** were co-cultured with *C. alb* SC5314 for 24 h at 0.03 μg mL^{-1}. Bars represent the mean $\pm$ SD (n = 3).

2.7. Prevented the morphological transition of *C. albicans* and inhibited fungal biofilm formation

The biofilm is a polysaccharide–protein complex secreted by fungi after forming a community and enveloping the fungal surface. Due to its natural barrier effect, it reduces drug uptake, leading to fungal drug resistance. Therefore, we investigated whether our target compounds have biofilm inhibition effects, thereby confirming the compound's anti-resistance mechanism. The yeast-to-hypha transition, also known as the filamentation of microbial colonies, is a crucial step in the formation of fungal biofilms. Consequently, we investigated the impact of the target molecule **A11** on fungal morphological transition, particularly during the yeast-to-hypha transition.
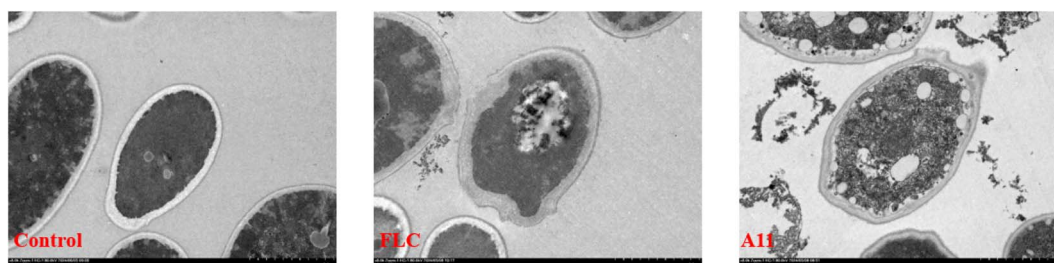

Fig. 4 Morphological observation of fungal cells (*C. alb* SC5314). **FLC** and **A11** were co-cultured with *C. alb* SC5314 for 24 h at 2 μg mL^{-1}.

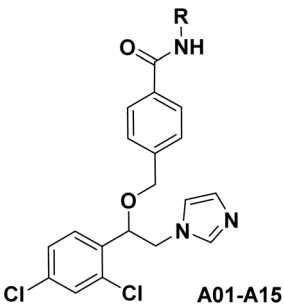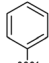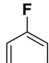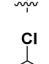**Table 2** The antifungal activity of the target compounds A01–A15
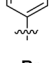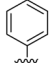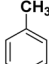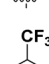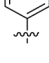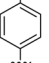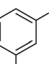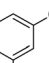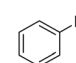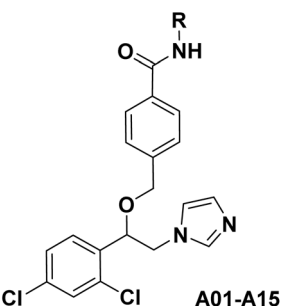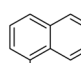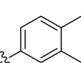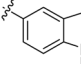
		MIC$_{80}$/(μg mL^{-1})				
Compd	R	Strain 904	Strain 901	Strain 632	Strain 17#	Strain CaR
A01		0.5	2	4	8	4
A02	F	0.25	4	4	8	8
A03	Cl	0.25	2	4	16	8
A04	Br	0.25	2	4	16	4
A05	CH$_3$	0.25	4	4	8	4
A06	CF$_3$	0.25	2	2	16	2
A07	OCH$_3$	0.25	4	4	4	4
A08	F	0.25	2	4	16	4
A09	Cl	0.25	2	4	8	8
A10	Br	0.25	2	8	16	8
A11	F, F	0.125	1	2	1	2
A12		2	8	8	8	4

Table 2 (Contd.)

		MIC$_{80}$/(μg mL^{-1})				
Compd	R	Strain 904	Strain 901	Strain 632	Strain 17#	Strain CaR
A13		1	1	8	64	128
A14		16	16	16	64	8
A15		8	8	128	>128	128
Fluconazole		>128	>128	>128	>128	>128

This analysis focused on understanding the underlying mechanisms involved in this transition. The experimental results were shown in Fig. 5.

The results of the study demonstrated that fluconazole did not inhibit the morphological transition in azole-resistant strain 904. Conversely, the introduction of the target compound **A11** at a concentration of 0.25 μg mL^{-1} completely hindered the morphogenetic transition of azole-resistant strain 904 from yeast to hyphae (as depicted in Fig. 5).

Subsequently, we also investigated the impact of the target compound on the formation of mature biofilms. As shown in Fig. 6, compound **A11** showed dose-dependent destruction of mature fungal biofilms of azole-resistant strain 904. These two experiments showed that **A11** can inhibit the initial transformation of yeast into mycelium and destroy mature biofilms.

2.8. Downregulated drug resistant gene

Our target compound showed good anti-resistance activity, which prompted us to investigate whether this was related to the expression of resistance genes. The resistance of *Candida albicans* to azole has been shown to be related to a variety of factors, such as the overexpression of *ERG11* or the upregulation of efflux pumps.[16,17] To investigate whether the anti-drug resistance mechanism of our target compounds is related to the two factors, the expression of the resistant gene *ERG11* and *CDR1* treated with drugs was determined by the real-time reverse transcriptase polymerase chain reaction (RT-PCR).
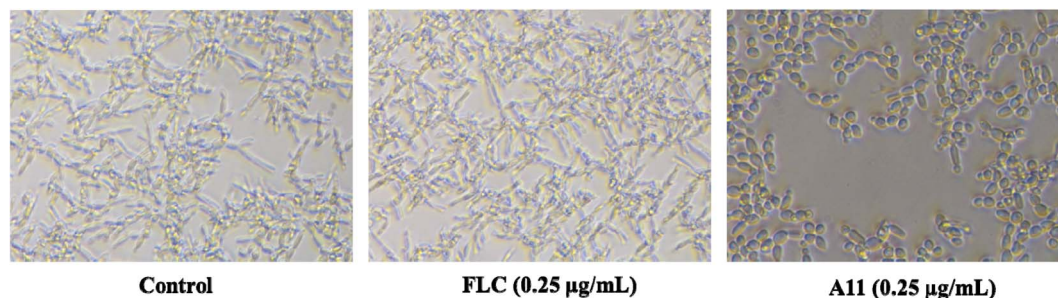
Fig. 5 DIC microscope photographs on the filamentation of azole-resistant strain 904. FLC and **A11** were co-cultured with strain 904 for 5 h at 0.25 μg mL^{-1}.
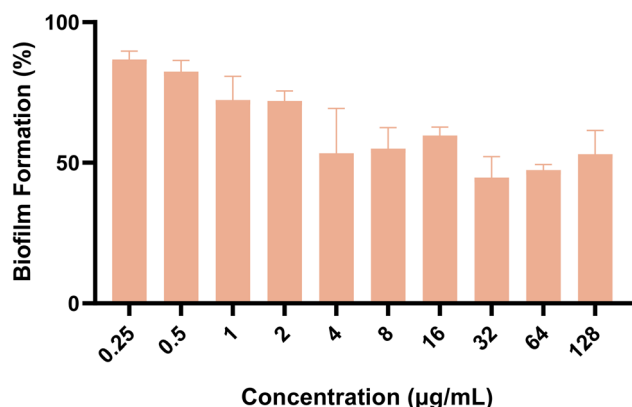
Fig. 6 The effect of compound **A11** on the biofilm formation (%) of azole-resistant strain 904. The outcomes were expressed as the average ± standard deviation *via* three separate trials.

From the obtained experimental results (Fig. 7), there was overexpression of drug resistance gene *ERG11* and *CDR1* after fluconazole treatment, which may be the cause of fluconazole resistance. When treated with the target compounds **A01**, **A07** and **A11**, the expression of these genes was reduced to basic levels. Overall, the resistance mechanism of our compounds is related to these two genes.

2.9. Minimum fungicidal concentration and time-kill tests

If a compound can completely eradicate fungi, especially resistant strains, it would be more valuable for development. Therefore, we have also conducted minimum fungicidal concentration testing and concentration-dependent time-kill assays for compound **A11** against strain 904.

As shown in Table 3, compound **A11** demonstrated significant fungicidal activity in this study, with MFC = 2 μg mL^{-1}. In the time-kill curve assay, gradient doses of compound **A11** (8 × MIC, 16 × MIC, 32 × MIC) and fluconazole (16 μg mL^{-1}) were tested. Compound **A11** exhibited potent fungicidal effects at three concentrations. Consequently, compound **A11** is expected to shorten the duration of treatment for invasive fungal infections (Fig. 8).

2.10. Analysis of changes in ROS level

Our target compounds not only exhibit fungistatic activity but also fungicidal activity. This result prompted us to investigate whether the compounds have a new mechanism of action. The generation of reactive oxygen species (ROS) has been reported to cause mitochondrial damage in fungi, leading to fungal death.[17] Therefore, we also investigated whether the target compounds can stimulate the production of reactive oxygen species, thereby demonstrating fungicidal activity. In detail, we employed the DCFH-DA method to examine the variations in ROS levels in strain 904 when exposed to compound **A11**.

Table 3 The minimum fungicidal concentration of compound **A11**[a]

Compd	MIC against *C. alb* (μg mL^{-1})	MFC against *C. alb* (μg mL^{-1})	MFC/MIC
A11	0.125	2	16
Fluconazole	>128	>128	—

[a] Abbreviations: *C. alb*, strain 904, fluconazole-resistant strain of *C. albicans*.
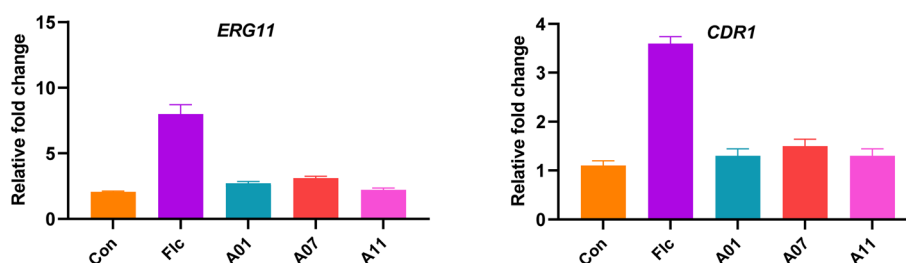
Fig. 7 Expression of resistant gene *ERG11* and *CDR1* of azole-resistant strain of *Candida albicans* (strain 904). The concentration of compounds and FLC was 0.25 μg mL^{-1} and DMSO as control. The outcomes were expressed as the average ± standard deviation *via* three separate trials.

Time-kill curve

Fig. 8 The time-kill curves of compound **A11**.

Fig. 9 Effect of compound **A11** on ROS in strain 904.

Fig. 9 demonstrates a significant increase in intracellular ROS levels when exposed to 0.25 μg mL^{-1} of **A11**, as compared to the blank and fluconazole experimental groups. The results s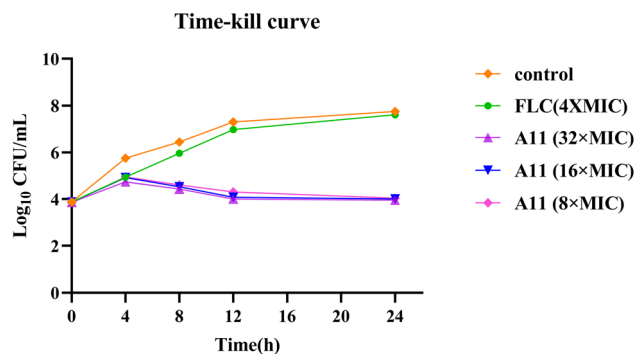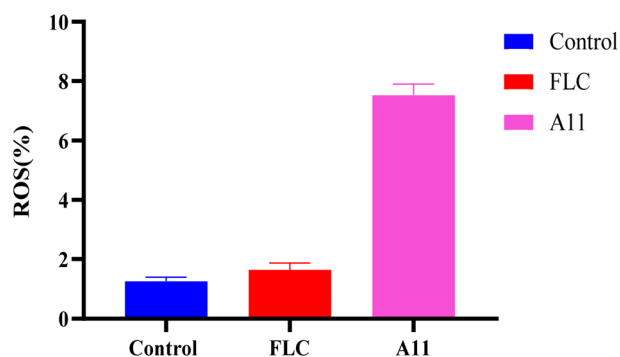howed the target compounds could enhance their antifungal effectiveness by inducing the substantial production of reactive oxygen species (ROS) within fungal cells.

2.11. Metabolic stability assay of liver microsomes

During the drug discovery process, the metabolic stability of lead compounds is a critical factor influencing their druggability. Therefore, we first evaluated the metabolic stability of the representative compound **A11** in liver microsomes, with miconazole selected as the positive control. The results are shown in the Table 4. Miconazole had a $T_{1/2}$ of 8.3 min, while the representative compound **A11** exhibited greater metabolic stability with a $T_{1/2}$ of 15.5 min.

2.12. Plasma stability assay

Despite the hepatic metabolic stability of a compound being widely regarded as one of the major challenges in the drug

Table 4 Metabolic stability of the representative compound A11

Compd	$T_{1/2}$ (min)	CL (mL min^{-1} mg^{-1})
A11	15.5	0.0894
Miconazole	8.3	0.6601
Fluconazole	>120	0.002

Table 5 Plasma stability of the representative compound A11

Compd	Time point (min)	% remaining	$T_{1/2}$ (min)
A11	180	73.9	>360
Miconazole	180	94.9	>360
Fluconazole	180	102	>360

discovery process, the plasma stability of the compound remains a significant influencing factor in new drug development. Since the metabolic enzymes in the liver differ from those in the blood, stability in liver microsomes *in vitro* does not necessarily indicate stability in plasma. Therefore, we also evaluated the plasma stability of the representative compound **A11**. The results are shown in the Table 5. The representative compound **A11** and positive drugs such as miconazole and fluconazole all demonstrated excellent plasma stability, with $T_{1/2}$ values exceeding 360 min. The results of liver microsomal metabolic stability and plasma metabolic stability indicated that the target compounds were valuable for further research and development.

2.13. *In vitro* cytotoxical effects on normal cells

Toxicity study on normal human cells is an important part of drug development. Therefore, we selected the human embryonic lung fibroblast cell (MRC-5) as model cell to evaluate the cytotoxicity of our compounds. The cells were treated with our compounds for 72 hours, and the results are presented in Table 6. We observed that the IC$_{50}$ values of compounds **A01–A15** were all greater than 100 μM. This suggests that compounds **A01–A15** did not exhibit any toxicity towards MRC-5 cells, indicating their safety in normal human cells.

2.14. *In vivo* efficiency of compound A11

Given the compound **A11**'s good *in vitro* antifungal activity, especially its significant inhibitory effect on resistant strains, we subsequently conducted *in vivo* activity studies on compound **A11**, with fluconazole being used as a positive control. In this experiment, a mouse model of azole-resistant strain 904 infection was established by injecting the resistant strain into the tail vein of mice. The effectiveness of compound **A11** in combating the infection was evaluated by assessing the colony-forming units (CFU) of the fungal burden in the kidneys of mice on the fifth day after infection. The results are shown in the Fig. 10.

Table 6 The IC$_{50}$ of compounds A01-A15 on MRC-5 cell lines

Compd	IC$_{50}$ (μM)	Compd	IC$_{50}$ (μM)
A01	>100	**A10**	>100
A02	>100	**A11**	>100
A03	>100	**A12**	>100
A04	>100	**A13**	>100
A05	>100	**A14**	>100
A06	>100	**A15**	>100
A07	>100	**Miconazole**	>100
A08	>100	**Fluconazole**	>100
A09	>100	***cis*-Pt**	78.3
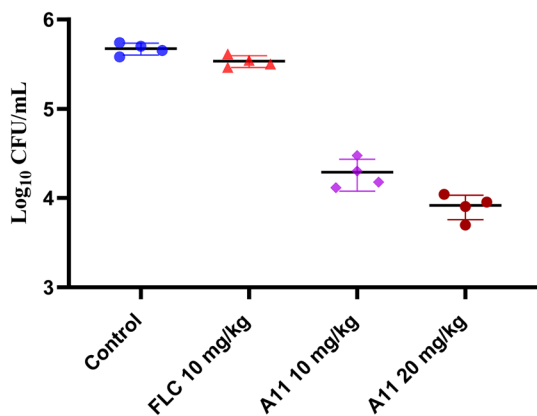
Fig. 10 Therapeutic efficacies of compound **A11** and fluconazole in the azole-resistant strain 904.

The results showed that compound **A11** also exhibited potent efficacy against the azole-resistant strain 904 *in vivo* (Fig. 10). In contrast, fluconazole was ineffective against azole-resistant strains *in vivo*. This result suggests that our target compound holds promise for treating infections caused by resistant fungi.

2.15. Molecular docking studies

Design strategies for target compounds were validated through molecular docking studies using *Candida albicans* CYP51 crystal structure (PDB code: 5TZ1) with compound **A11**, conducted *via* Discovery Studio 3.0. Miconazole, an imidazole drug, served as a control (Fig. 11). Results illustrated interactions between the imidazole group of compound **A11** and miconazole with the iron of the heme group. Moreover, the chlorophenyl group of compound **A11** fit snugly within hydrophobic pocket I formed
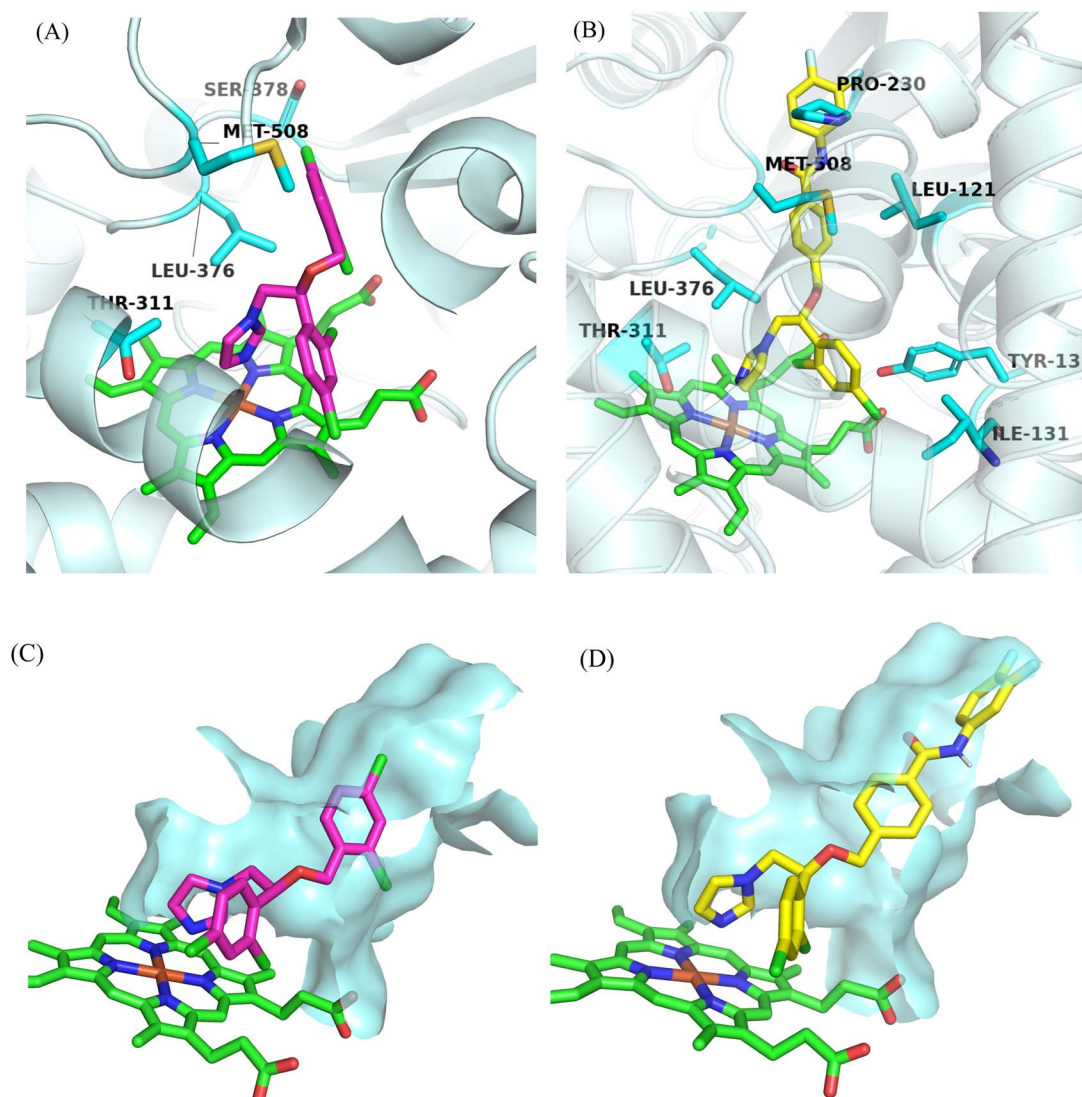
Fig. 11 Predicted binding mode of (A) MCZ, (B) **A11** with *Candida albicans* CYP51. Binding conformation of (C) MCZ, (D) **A11** in the active pocket of *Candida albicans* CYP51.

by ILE131 and TYR132. Furthermore, the other dichlorobenzene of miconazole interacts solely with Met508 at the entrance of hydrophobic channel II. However, the benzanilide fragment of target compound **A11** can deeply insert into the narrow hydrophobic channel II, which is composed of MET508, LEU121 and PRO230.

3. Conclusion

Severe fungal infections pose a significant threat to human health, and the global incidence of deep fungal infections is on the rise. Furthermore, the increasing use of antifungal medications has contributed to the emergence of drug-resistant strains, exacerbating the problem. Consequently, there is an urgent need to develop novel antifungal drugs with unique structures to effectively combat drug-resistant fungal infections. In this study, a series of novel benzanilide-containing azoles have been designed. In particular, the hydrophobic benzanilide rings was expected to penetrate deep into narrow hydrophobic channels II of CYP51, thereby enhancing antifungal activity. Then, the new derivatives were synthesized and their structures were analyzed by ^{1}H NMR, ^{13}C-NMR, and HRMS spectral. And the compounds **A01–A15** were screened for *in vitro* antifungal activity against *Candida albicans* (SC5314), *Candida parapsilosis*, *Candida glabrata*, *Candida krusei* and *Cryptococcus neoformans*. Intriguingly, all the target compounds showed moderate to exceptional efficacy against the five fluconazole-sensitive *Candida albicans*. Further investigation demonstrated that compound **A11**, the most potent among the synthesized derivatives, exhibits significant antifungal activity by inhibiting the fungal CYP51 enzyme and suppressing fungal ergosterol production. Meantime, the direct observation of cell membrane damage further confirmed that the target of our compound is CYP51. Most interesting is that the target compounds displayed notable activity against fluconazole-resistant strains, surpassing the efficacy of the positive control drug fluconazole. Meanwhile, investigations into the mechanisms of drug resistance unveiled that the compounds were capable of suppressing the formation of biofilm and the expression of the resistance-related gene *ERG11* and the efflux pumps gene *CDR1*, consequently reversing drug resistance. Moreover, compound **A11** exhibited fungicide effects against fluconazole-resistant strain and notably increased the intracellular ROS level, leading to cellular harm. Compound **A11** also demonstrated good liver microsomal stability ($T_{1/2} = 15.5$ min) and plasma stability ($T_{1/2} > 360$ min). In addition, these compounds also showed low toxicity towards human MRC-5 cell with $IC_{50} > 100$ μM, indicating their potential as safe and effective antifungal agents. In a mouse infection model, mice treated with **A11** for infection showed a significantly reduced fungal burden compared to mice treated with FLC. Molecular docking experiment demonstrated compound **A11** can form a strong binding interaction with *Candida albicans* CYP51. Specifically, the benzanilide fragment can penetrate deeply into the narrow hydrophobic channel II, thereby achieving the intended design goal. These findings suggest that the novel benzanilide-containing azoles could be promising candidates for the treatment of drug-resistant fungal infections.

4. Experimental

4.1. Chemistry

All reagents and solvents used in the study were purchased from commercial suppliers and used as received without further purification. Silica gel (200–300 mesh) was used for column chromatography, and silica gel precoated GF254 plates were used for TLC analysis. Melting points were measured using an X-5 melting point equipment from Beijing Tech Instrument Co., Ltd, Beijing, China. High-resolution mass spectra (HRMS) were recorded using an Agilent Accurate-Mass Q-TOF 6530 instrument (Santa Clara, CA, USA) in ESI mode. ^{1}H NMR and ^{13}C NMR spectra were recorded in DMSO-d_6 solvent on a 400 (100)-MHz Bruker AV-400 spectrometer (Bruker Bioscience, Billerica, MA, USA).

4.2. General procedure for the synthesis of target compounds A01–A15

The synthesis of target compound 4-((1-(2,4-dichlorophenyl)-2-(1*H*-imidazol-1-yl)ethoxy)methyl)-*N*-phenylbenzamide (**A01**) was chosen as the example: 2-bromo-1-(2,4-dichlorophenyl)ethan-1-one (5.32 g, 20 mmol) and imidazole (1.50 g, 22 mmol) are added to a solution of methanol (20 mL), followed by the addition of triethylamine (2.02 g, 20 mmol), and refluxed for 4 hours. The solvent was removed under reduced pressure, and 20 mL of water was added. The mixture was then extracted with ethyl acetate (3 × 10 mL), and the combined organic phase was sequentially washed with water (3 × 10 mL) and saturated brine (20 mL). After drying over anhydrous sodium sulfate and filtering the drying agent, the crude product was obtained by vacuum concentration. The crude product was purified by column chromatography (petroleum ether : ethyl acetate = 2 : 1) to afford intermediate **3** (4.12 g) as a yellow solid with a yield of 90.0%. Subsequently, compound **3** (4.12 g, 18 mmol) was dissolved in methanol (30 mL), followed by the portion-wise addition of sodium borohydride (0.68 g, 18 mmol), and the mixture was stirred at room temperature for 2 hours. After the reaction was completed, water (50 mL) was added, and the reaction mixture was extracted three times with ethyl acetate (3 × 20 mL). The combined organic layers were concentrated under reduced pressure. The crude product was purified by column chromatography (petroleum ether : ethyl acetate = 4 : 1) to obtain the key intermediate **4** (3.67 g) with a yield of 80.0%. Intermediate **4** (3.67 g, 14.4 mmol) and 4-(bromomethyl)benzoate (3.28 g, 14.4 mmol) were added to tetrahydrofuran (30 mL), followed by the portion-wise addition of sodium hydride (0.5 g), and the reaction was carried out at 70 °C for 4 hours. After the reaction was completed, water (50 mL) was added, and the reaction mixture was extracted three times with ethyl acetate (3 × 20 mL). The combined organic layers were concentrated under reduced pressure. The crude product was purified by column chromatography (petroleum ether : ethyl acetate = 8 : 1) to obtain the key intermediate **5** (3.81 g) with a yield of 65.5%. Intermediate **5** (0.38 g, 0.94 mmol) was dissolved in methanol (10 mL), and potassium hydroxide (0.05 g, 0.94 mmol) was added, followed by heating under reflux for 1 hour. After the

reaction was completed, the reaction mixture was concentrated and, without further purification, directly dissolved in dichloromethane. EDCI (0.18 g, 0.94 mmol) and DMAP (0.06 g, 0.47 mmol) were then added, followed by the addition of aniline (0.09 g, 0.94 mmol), and the reaction was allowed to proceed at room temperature for 1 hour. After the reaction was completed, water (50 mL) was added, and the reaction mixture was extracted three times with ethyl acetate (3 × 10 mL). The combined organic layers were concentrated under reduced pressure. The crude product was purified by column chromatography (petroleum ether : ethyl acetate = 8 : 1) to obtain the final product **A01** (0.36 g) by column chromatography with a two-step yield of 82.0%. m.p. 132.4–134.3 °C. HRMS (ESI): calcd for $C_{25}H_{21}N_3O_2Cl_2$ [M + H]$^+$: 466.1084, found 466.1100 [M + H]$^+$. ^{1}H NMR (400 MHz, DMSO-d_6) δ 10.22 (s, 1H), 7.91 (d, J = 8.3 Hz, 2H), 7.80–7.77 (m, 2H), 7.69 (d, J = 2.1 Hz, 1H), 7.53 (s, 1H), 7.50 (dd, J = 8.4, 2.1 Hz, 1H), 7.43 (d, J = 8.4 Hz, 1H), 7.38–7.33 (m, 2H), 7.31 (d, J = 8.3 Hz, 2H), 7.12–7.08 (m, 2H), 6.90 (s, 1H), 5.05 (dd, J = 7.0, 3.8 Hz, 1H), 4.54–4.38 (m, 2H), 4.36–4.25 (m, 2H). ^{13}C NMR (100 MHz, DMSO-d_6) δ 165.7, 141.7, 139.6, 138.4, 135.2, 134.6, 134.1, 133.7, 129.8, 129.5, 129.1, 128.7, 128.4, 128.2, 127.4, 124.1, 120.9, 120.6, 77.1, 70.3, 50.5. The preparation methods of target compounds **A02–A15** were the same as that of target compound **A01**.

4.2.1. 4-((1-(2,4-Dichlorophenyl)-2-(1H-imidazol-1-yl) ethoxy)methyl)-N-(4-fluorophenyl)benzamide (A02). White solid (88.1% yield); m.p. 139.1–141.3 °C. HRMS (ESI): calcd for $C_{25}H_{20}N_3O_2Cl_2F$ [M + Na]$^+$: 506.0809, found 506.0837 [M + Na]$^+$. ^{1}H NMR (400 MHz, DMSO-d_6) δ 10.28 (s, 1H), 7.90 (d, J = 8.4 Hz, 2H), 7.80 (dd, J = 9.2, 5.1 Hz, 2H), 7.69 (d, J = 2.1 Hz, 1H), 7.54 (s, 1H), 7.50 (dd, J = 8.4, 2.1 Hz, 1H), 7.43 (d, J = 8.3 Hz, 1H), 7.31 (d, J = 8.3 Hz, 2H), 7.20 (t, J = 8.9 Hz, 2H), 7.08 (s, 1H), 6.90 (s, 1H), 5.04 (dd, J = 7.0, 3.8 Hz, 1H), 4.55–4.38 (m, 2H), 4.36–4.25 (m, 2H). ^{13}C NMR (100 MHz, DMSO-d_6) δ 165.6, 160.0, 157.6, 141.8, 138.4, 136.0, 135.9, 135.2, 134.4, 134.1, 133.7, 129.8, 129.5, 128.7, 128.4, 128.2, 127.4, 122.7, 122.6, 120.6, 115.8, 115.5, 77.1, 70.3, 50.5.

4.2.2. N-(4-Chlorophenyl)-4-((1-(2,4-dichlorophenyl)-2-(1H-imidazol-1-yl)ethoxy)methyl)benzamide (A03). White solid (86.3% yield); m.p. 141.4–143.4 °C. HRMS (ESI): calcd for $C_{25}H_{20}N_3O_2Cl_3$ [M + Na]$^+$: 522.0513, found 522.0539 [M + Na]$^+$. ^{1}H NMR (400 MHz, DMSO-d_6) δ 10.35 (s, 1H), 7.90 (d, J = 8.3 Hz, 2H), 7.83 (d, J = 8.9 Hz, 2H), 7.69 (d, J = 2.1 Hz, 1H), 7.54 (s, 1H), 7.50 (dd, J = 8.4, 2.1 Hz, 1H), 7.44–7.41 (m, 2H), 7.40 (d, J = 2.1 Hz, 1H), 7.32 (d, J = 8.3 Hz, 2H), 7.09 (s, 1H), 6.90 (s, 1H), 5.04 (dd, J = 6.9, 3.8 Hz, 1H), 4.55–4.38 (m, 2H), 4.36–4.25 (m, 2H). ^{13}C NMR (100 MHz, DMSO-d_6) δ 165.8, 141.9, 138.6, 135.2, 134.3, 134.1, 133.7, 129.8, 129.5, 129.0, 128.7, 128.4, 128.2, 127.7, 127.4, 122.3, 77.1, 70.3, 50.5.

4.2.3. N-(4-Bromophenyl)-4-((1-(2,4-dichlorophenyl)-2-(1H-imidazol-1-yl)ethoxy)methyl)benzamide (A04). White solid (83.2% yield); m.p. 139.1–141.3 °C. HRMS (ESI): calcd for $C_{25}H_{20}N_3O_2Cl_2Br$ [M + Na]$^+$: 566.0008, found 566.0018 [M + Na]$^+$. ^{1}H NMR (400 MHz, DMSO-d_6) δ 10.35 (s, 1H), 7.90 (d, J = 8.3 Hz, 2H), 7.78 (d, J = 8.9 Hz, 2H), 7.69 (d, J = 2.1 Hz, 1H), 7.55 (d, J = 2.1 Hz, 1H), 7.54–7.52 (m, 2H), 7.50 (dd, J = 8.4, 2.1 Hz, 1H), 7.43 (d, J = 8.4 Hz, 1H), 7.32 (d, J = 8.3 Hz, 2H), 7.08 (s, 1H), 6.90 (s, 1H), 5.04 (dd, J = 7.0, 3.9 Hz, 1H), 4.54–4.38 (m, 2H), 4.36–4.25 (m, 2H). ^{13}C NMR (100 MHz, DMSO-d_6) δ 165.8, 141.9, 139.01, 138.4, 135.2, 134.3, 134.1, 133.7, 131.9, 129.8, 129.5, 128.7, 128.4, 128.2, 127.4, 122.7, 120.6, 115.8, 77.1, 70.3, 50.5.

4.2.4. 4-((1-(2,4-Dichlorophenyl)-2-(1H-imidazol-1-yl) ethoxy)methyl)-N-(p-tolyl)benzamide (A05). White solid (84.5% yield); m.p. 134.7–136.4 °C. HRMS (ESI): calcd for $C_{26}H_{23}N_3O_2Cl_2$ [M + Na]$^+$: 502.1060, found 502.1080 [M + Na]$^+$. ^{1}H NMR (400 MHz, DMSO-d_6) δ 10.14 (s, 1H), 7.90 (d, J = 8.2 Hz, 2H), 7.68 (d, J = 2.1 Hz, 1H), 7.66 (d, J = 8.4 Hz, 2H), 7.53 (s, 1H), 7.50 (dd, J = 8.4, 2.1 Hz, 1H), 7.43 (d, J = 8.4 Hz, 1H), 7.30 (d, J = 8.0 Hz, 2H), 7.15 (d, J = 8.3 Hz, 2H), 7.08 (s, 1H), 6.90 (s, 1H), 5.04 (dd, J = 7.0, 3.8 Hz, 1H), 4.54–4.38 (m, 2H), 4.36–4.25 (m, 2H), 2.28 (s, 3H). ^{13}C NMR (100 MHz, DMSO-d_6) δ 165.4, 141.6, 138.4, 137.1, 135.3, 134.6, 134.1, 133.7, 133.1, 129.8, 129.5, 129.4, 128.7, 128.4, 128.1, 127.4, 120.9, 120.6, 77.1, 70.3, 50.5, 21.0.

4.2.5. 4-((1-(2,4-Dichlorophenyl)-2-(1H-imidazol-1-yl) ethoxy)methyl)-N-(4-(trifluoromethyl)phenyl)benzamide (A06). White solid (86.9% yield); m.p. 137.6–139.2 °C. HRMS (ESI): calcd for $C_{26}H_{20}N_3O_2Cl_2F_3$ [M + Na]$^+$: 556.0777, found 556.0809 [M + Na]$^+$. ^{1}H NMR (400 MHz, DMSO-d_6) δ 10.57 (s, 1H), 8.03 (d, J = 8.5 Hz, 2H), 7.93 (d, J = 8.3 Hz, 2H), 7.73 (d, J = 8.8 Hz, 2H), 7.69 (d, J = 2.1 Hz, 1H), 7.54 (s, 1H), 7.50 (dd, J = 8.4, 2.1 Hz, 1H), 7.43 (d, J = 8.4 Hz, 1H), 7.34 (d, J = 8.3 Hz, 2H), 7.09 (s, 1H), 6.90 (s, 1H), 5.05 (dd, J = 7.0, 3.8 Hz, 1H), 4.57–4.38 (m, 2H), 4.39–4.24 (m, 2H). ^{13}C NMR (100 MHz, DMSO-d_6) δ 166.2, 143.3, 142.1, 138.4, 135.2, 134.1, 133.7, 129.8, 129.5, 128.4, 127.5, 126.4, 126.4, 124.3, 123.9, 123.5, 120.6, 77.1, 70.3, 50.5.

4.2.6. 4-((1-(2,4-Dichlorophenyl)-2-(1H-imidazol-1-yl) ethoxy)methyl)-N-(4-methoxyphenyl)benzamide (A07). White solid (81.5% yield); m.p. 144.6–146.3 °C. HRMS (ESI): calcd for $C_{26}H_{23}N_3O_3Cl_2$ [M + Na]$^+$: 518.1009, found 518.1030 [M + Na]$^+$. ^{1}H NMR (400 MHz, DMSO-d_6) δ 10.11 (s, 1H), 7.90 (d, J = 8.2 Hz, 2H), 7.69 (d, J = 1.9 Hz, 1H), 7.68 (d, J = 5.3 Hz, 2H), 7.53 (s, 1H), 7.50 (dd, J = 8.4, 2.1 Hz, 1H), 7.43 (d, J = 8.4 Hz, 1H), 7.30 (d, J = 8.0 Hz, 2H), 7.08 (s, 1H), 6.93 (d, J = 9.0 Hz, 2H), 6.90 (s, 1H), 5.04 (dd, J = 7.0, 3.9 Hz, 1H), 4.54–4.38 (m, 2H), 4.36–4.25 (m, 2H), 3.75 (s, 3H). ^{13}C NMR (100 MHz, DMSO-d_6) δ 165.2, 156.0, 141.5, 138.4, 135.2, 134.6, 134.1, 133.7, 132.7, 129.8, 129.5, 128.7, 128.4, 128.1, 127.4, 122.4, 120.6, 114.2, 77.1, 70.3, 55.6, 50.5.

4.2.7. 4-((1-(2,4-Dichlorophenyl)-2-(1H-imidazol-1-yl) ethoxy)methyl)-N-(3-fluorophenyl)benzamide (A08). White solid (86.2% yield); m.p. 137.8–139.5 °C. HRMS (ESI): calcd for $C_{25}H_{20}N_3O_2Cl_2F$ [M + Na]$^+$: 506.0809, found 506.0824 [M + Na]$^+$. ^{1}H NMR (400 MHz, DMSO-d_6) δ 10.41 (s, 1H), 7.92–7.88 (m, 2H), 7.77 (dt, J = 11.8, 2.3 Hz, 1H), 7.69 (d, J = 2.1 Hz, 1H), 7.57 (dd, J = 8.2, 1.1 Hz, 1H), 7.53 (d, J = 1.1 Hz, 1H), 7.50 (dd, J = 8.4, 2.1 Hz, 1H), 7.44–7.36 (m, 2H), 7.33 (d, J = 8.3 Hz, 2H), 7.09 (s, 1H), 6.90 (d, J = 1.1 Hz, 1H), 5.05 (dd, J = 7.0, 3.9 Hz, 1H), 4.56–4.39 (m, 2H), 4.36–4.24 (m, 2H). ^{13}C NMR (100 MHz, DMSO-d_6) δ 165.9, 163.7, 161.4, 142.0, 141.5, 141.4, 138.4, 135.2, 134.2, 134.1, 133.7, 130.7, 130.7, 129.8, 129.5, 128.7, 128.4, 128.2, 127.5, 120.6, 116.5, 116.4, 110.7, 110.5, 107.6, 107.3, 77.1, 70.3, 50.5.

4.2.8. N-(3-Chlorophenyl)-4-((1-(2,4-dichlorophenyl)-2-(1H-imidazol-1-yl)ethoxy)methyl)benzamide (A09). White solid

(88.0% yield); m.p. 129.6–131.8 °C. HRMS (ESI): calcd for $C_{25}H_{20}N_3O_2Cl_3$ [M + Na]$^+$: 522.0513, found 522.0507 [M + Na]$^+$. ^{1}H NMR (400 MHz, DMSO-d_6) δ 10.38 (s, 1H), 7.98 (t, J = 2.1 Hz, 1H), 7.91 (d, J = 8.3 Hz, 2H), 7.72 (dd, J = 7.7, 1.8 Hz, 1H), 7.69 (d, J = 2.1 Hz, 1H), 7.54 (s, 1H), 7.50 (dd, J = 8.4, 2.1 Hz, 1H), 7.40 (dd, J = 20.4, 8.3 Hz, 2H), 7.33 (d, J = 8.1 Hz, 2H), 7.16 (dd, J = 8.0, 1.2 Hz, 1H), 7.09 (s, 1H), 6.90 (s, 1H), 5.05 (dd, J = 7.0, 3.8 Hz, 1H), 4.55–4.39 (m, 2H), 4.36–4.25 (m, 2H). ^{13}C NMR (100 MHz, DMSO-d_6) δ 165.9, 142.0, 141.1, 138.4, 135.2, 134.1, 134.1, 133.7, 133.4, 130.8, 129.8, 129.5, 128.7, 128.4, 128.3, 127.5, 123.8, 120.6, 120.2, 119.1, 77.1, 70.3, 50.5.

4.2.9. ***N*-(3-Bromophenyl)-4-((1-(2,4-dichlorophenyl)-2-(1*H*-imidazol-1-yl)ethoxy)methyl)benzamide (A10).** White solid (82.4% yield); m.p. 136.1–138.3 °C. HRMS (ESI): calcd for $C_{25}H_{20}N_3O_2Cl_2Br$ [M + Na]$^+$: 566.0008, found 566.0020 [M + Na]$^+$. ^{1}H NMR (400 MHz, DMSO-d_6) δ 10.37 (s, 1H), 8.12 (t, J = 2.0 Hz, 1H), 7.91 (d, J = 8.3 Hz, 2H), 7.77 (dt, J = 7.7, 1.8 Hz, 1H), 7.68 (d, J = 2.1 Hz, 1H), 7.56–7.53 (m, 1H), 7.50 (dd, J = 8.4, 2.1 Hz, 1H), 7.43 (d, J = 8.4 Hz, 1H), 7.34–7.30 (m, 4H), 7.09 (s, 1H), 6.90 (s, 1H), 5.05 (dd, J = 7.0, 3.8 Hz, 1H), 4.55–4.38 (m, 2H), 4.36–4.25 (m, 2H). ^{13}C NMR (100 MHz, DMSO-d_6) δ 165.9, 142.0, 141.3, 138.4, 135.2, 134.1, 134.1, 133.7, 131.1, 129.8, 129.5, 128.7, 128.4, 128.3, 127.4, 126.7, 123.0, 121.9, 120.6, 119.5, 77.1, 70.3, 50.5.

4.2.10. 4-((1-(2,4-Dichlorophenyl)-2-(1*H*-imidazol-1-yl)ethoxy)methyl)-*N*-(2,4-difluorophenyl)benzamide (A11). White solid (81.7% yield); m.p. 141.0–143.4 °C. HRMS (ESI): calcd for $C_{25}H_{19}N_3O_2Cl_2F_2$ [M + Na]$^+$: 524.0715, found 524.0722 [M + Na]$^+$. ^{1}H NMR (600 MHz, DMSO-d_6) δ 10.12 (s, 1H), 7.92 (d, J = 8.4 Hz, 2H), 7.69 (d, J = 2.1 Hz, 1H), 7.59 (td, J = 8.9, 6.2 Hz, 1H), 7.53 (d, J = 1.1 Hz, 1H), 7.50 (dd, J = 8.4, 2.1 Hz, 1H), 7.43 (d, J = 8.4 Hz, 1H), 7.36 (ddd, J = 10.6, 9.1, 2.8 Hz, 1H), 7.31 (d, J = 8.2 Hz, 2H), 7.16–7.10 (m, 1H), 7.08 (t, J = 1.2 Hz, 1H), 6.89 (d, J = 1.1 Hz, 1H), 5.04 (dd, J = 7.0, 3.9 Hz, 1H), 4.56–4.38 (m, 2H), 4.35–4.25 (m, 2H). ^{13}C NMR (100 MHz, DMSO-d_6) δ 165.6, 161.3, 159.0, 158.9, 157.9, 157.8, 155.4, 155.3, 142.1, 138.4, 135.2, 134.1, 133.7, 133.3, 129.9, 129.5, 129.1, 129.1, 129.0, 128.9, 128.7, 128.4, 128.3, 127.5, 122.8, 122.7, 122.7, 120.6, 111.8, 111.8, 111.6, 111.5, 105.1, 104.9, 104.6, 77.1, 70.3, 50.5.

4.2.11. 4-((1-(2,4-Dichlorophenyl)-2-(1*H*-imidazol-1-yl)ethoxy)methyl)-*N*-(quinolin-7-yl)benzamide (A12). White solid (87.6% yield); m.p. 133.6–136.1 °C. HRMS (ESI): calcd for $C_{28}H_{22}N_4O_2Cl_2$ [M + Na]$^+$: 539.1012, found 539.1028 [M + Na]$^+$. ^{1}H NMR (400 MHz, DMSO-d_6) δ 10.56 (s, 1H), 8.82 (dd, J = 4.2, 1.7 Hz, 1H), 8.56 (d, J = 2.3 Hz 1H), 8.33 (dd, J = 8.5, 1.7 Hz, 1H), 8.08–8.00 (m, 2H), 7.99–7.96 (m, 2H), 7.70 (d, J = 2.1 Hz, 1H), 7.55 (d, J = 1.1 Hz, 1H), 7.53–7.49 (m, 2H), 7.44 (d, J = 8.4 Hz, 1H), 7.35 (d, J = 8.3 Hz, 2H), 7.10 (s, 1H), 6.91 (s, 1H), 5.06 (dd, J = 7.0, 3.9 Hz, 1H), 4.56–4.41 (m, 2H), 4.37–4.27 (m, 2H). ^{13}C NMR (100 MHz, DMSO-d_6) δ 166.1, 149.7, 145.4, 142.0, 138.4, 137.6, 136.1, 135.2, 134.3, 134.1, 133.7, 132.2, 132.0, 129.8, 129.5, 129.1, 128.7, 128.4, 128.3, 127.5, 124.8, 122.2, 120.6, 116.8, 77.1, 70.3, 50.5.

4.2.12. 4-((1-(2,4-Dichlorophenyl)-2-(1*H*-imidazol-1-yl)ethoxy)methyl)-*N*-(naphthalen-1-yl)benzamide (A13). White solid (84.1% yield); m.p. 143.1–145.1 °C. HRMS (ESI): calcd for $C_{29}H_{23}N_3O_2Cl_2$ [M + Na]$^+$: 538.1060, found 538.1075 [M + Na]$^+$.

^{1}H NMR (400 MHz,) δ 10.42 (s, 1H), 8.04 (d, J = 8.2 Hz, 2H), 8.00–7.96 (m, 2H), 7.87 (d, J = 7.5 Hz, 1H), 7.70 (d, J = 2.1 Hz, 1H), 7.63–7.60 (m, 1H), 7.58–7.54 (m, 4H), 7.51 (dd, J = 8.4, 2.1 Hz, 1H), 7.44 (d, J = 8.4 Hz, 1H), 7.35 (d, J = 8.3 Hz, 2H), 7.10 (t, J = 1.2 Hz, 1H), 6.91 (t, J = 1.1 Hz, 1H), 5.07 (dd, J = 6.9, 3.9 Hz, 1H), 4.57–4.41 (m, 2H), 4.37–4.26 (m, 2H). ^{13}C NMR (100 MHz, DMSO-d_6) δ 166.3, 141.8, 138.4, 135.3, 134.3, 134.3, 134.1, 133.7, 129.9, 129.7, 129.5, 128.7, 128.6, 128.4, 128.3, 127.5, 126.8, 126.6, 126.5, 126.0, 124.4, 123.8, 120.6, 77.1, 70.3, 50.5.

4.2.13. 4-((1-(2,4-Dichlorophenyl)-2-(1*H*-imidazol-1-yl)ethoxy)methyl)-*N*-(naphthalen-2-yl)benzamide (A14). White solid (85.4% yield); m.p. 144.4–146.5 °C. HRMS (ESI): calcd for $C_{29}H_{23}N_3O_2Cl_2$ [M + Na]$^+$: 538.1066, found 538.1074 [M + Na]$^+$. ^{1}H NMR (400 MHz, DMSO-d_6) δ 10.44 (s, 1H), 8.47 (d, J = 2.0 Hz, 1H), 7.97 (d, J = 8.3 Hz, 2H), 7.92–7.83 (m, 4H), 7.69 (d, J = 2.1 Hz, 1H), 7.55 (s, 1H), 7.50 (td, J = 7.7, 7.1, 1.7 Hz, 2H), 7.46–7.41 (m, 2H), 7.34 (d, J = 8.3 Hz, 2H), 7.09 (d, J = 1.3 Hz, 1H), 6.91 (d, J = 1.1 Hz, 1H), 5.06 (dd, J = 7.0, 3.9 Hz, 1H), 4.56–4.40 (m, 2H), 4.37–4.26 (m, 2H). ^{13}C NMR (100 MHz, DMSO-d_6) δ 165.9, 141.8, 138.4, 137.3, 135.3, 134.5, 134.1, 133.8, 133.7, 130.5, 129.8, 129.5, 128.7, 128.6, 128.4, 128.3, 127.9, 127.9, 127.5, 126.9, 125.3, 121.5, 120.6, 117.1, 77.1, 70.3, 50.5.

4.2.14. 4-((1-(2,4-Dichlorophenyl)-2-(1*H*-imidazol-1-yl)ethoxy)methyl)-*N*-(1*H*-indol-5-yl)benzamide (A15). White solid (83.3% yield); m.p. 128.7–130.8 °C. HRMS (ESI): calcd for $C_{27}H_{22}N_4O_2Cl_2$ [M + Na]$^+$: 527.1012, found 527.1033 [M + Na]$^+$. ^{1}H NMR (400 MHz, DMSO-d_6) 11.04 (s, 1H), 10.06 (s, 1H), 7.99 (d, J = 1.9 Hz, 1H), 7.93 (d, J = 8.1 Hz, 2H), 7.69 (d, J = 2.1 Hz, 1H), 7.54 (s, 1H), 7.50 (dd, J = 8.4, 2.1 Hz, 1H), 7.45–7.39 (m, 2H), 7.37–7.32 (m, 2H), 7.31 (d, J = 8.2 Hz, 2H), 7.09 (s, 1H), 6.90 (s, 1H), 6.44–6.39 (m, 1H), 5.05 (dd, J = 7.0, 3.9 Hz, 1H), 4.54–4.38 (m, 2H), 4.36–4.26 (m, 2H). ^{13}C NMR (100 MHz, DMSO-d_6) δ 165.2, 141.2, 138.4, 135.3, 135.1, 134.1, 133.7, 133.5, 131.4, 129.8, 129.5, 128.7, 128.4, 128.1, 127.9, 127.4, 126.4, 120.6, 116.6, 112.7, 111.5, 101.6, 77.1, 70.4, 50.5.

4.3. *In vitro* antifungal assay

For antifungal assessment, the CLSI M27-A3 micro broth dilution assay was utilized. Compounds and controls were dissolved in DMSO, with RPM1640 medium added to 96-well plates. Tween-20 was used for stabilization. Each well received specific volumes of stock solutions, with fungal suspensions (1×10^3–5×10^3 CFU mL^{-1}) added before incubation at 35 °C to determine MIC.

4.4. GC-MS analysis of sterol composition

GC-MS analysis of sterol composition utilized *Candida albicans* (SC5314) in YEPD medium. After incubation and activation, fungal cells were saponified using a 15% sodium hydroxide solution in ethanol/water, followed by extraction with petroleum ether. Samples were then dissolved in cyclohexane and analyzed by GC-MS.

4.5. Experiment of transmission electron microscopy (TEM)

For transmission electron microscopy (TEM), *Candida albicans* SC5314 was treated with compounds and controls, incubated, fixed, and observed under TEM as per established methods.

4.6. RT-PCR assay

The RT-PCR analyses were performed following the methods outlined in earlier studies.[18]

4.7. Metabolic stabilities assay

The metabolic stability of the target compounds, encompassing liver microsomal and plasma stability, was evaluated using established experimental protocols from previous reports.[18] The liver microsomes were extracted from mouse. The plasma was collected from adult male SD rats.

4.8. *In vivo* antifungal potency

All animal procedures were performed in accordance with the Guidelines for Care and Use of Laboratory Animals of Zhengzhou University and approved by the Animal Ethics Committee of Zhengzhou University. To establish the *Candida albicans* infection model, mice were intravenously injected with a suspension of *C. alb* 904 (1×10^5 CFU mL^{-1}, 100 μL) into the tail vein. Intraperitoneal administration of the compounds followed 2 hours post-infection. After 5 days, the left kidneys of the mice were aseptically excised, pulverized, and spread on PDA plates to quantify colony-forming units (CFUs), assessing the fungal burden.

4.9. Cytotoxicity assay

The MRC-5 cell line used in this study was obtained from the American Type Culture Collection (ATCC). The cytotoxicity assay was performed following the methods outlined in earlier studies.[18]

4.10. Docking study

The crystal structure of CYP51 (PDB: 5TZ1) was obtained from the Protein Data Bank and optimized. Molecular docking was performed to simulate the interaction of the target molecule with the protein by using Discovery Studio 3.0 software. Docking results were analyzed graphically using PyMOL software.

Data availability

All relevant data are within the manuscript and its additional files.

Conflicts of interest

The authors have stated that they have no competing financial interests or personal relationships that could have influenced the work reported in this paper.

Acknowledgements

References

1 C. F. Neoh, W. Jeong, D. C. Kong and M. A. Slavin, *Expert Rev. Anti-Infect. Ther.*, 2023, **21**, 577–594.

2 D. A. Enoch, H. Yang, S. H Aliyu and C. Micallef, *Methods Mol. Biol.*, 2017, **1508**, 17–65.

3 K. C. Howard, E. K. Dennis, D. S. Watt and S. Garneau-Tsodikova, *Chem. Soc. Rev.*, 2020, **49**, 2426–2480.

4 D. Allen, D. Wilson, R. Drew and J. Perfect, *Expert Rev. Anti-Infect. Ther.*, 2015, **13**, 787–798.

5 S. Seyedmousavi, H. Rafati, M. Ilkit, A. Tolooe, M. T. Hedayati and P. Verweij, *Methods Mol. Biol.*, 2017, **1508**, 107–139.

6 X. Cui, L. Wang, Y. Lü and C. Yue, *J Infect Public Health*, 2022, **15**, 986–1000.

7 T. Y. Hargrove, L. Friggeri, Z. Wawrzak, A. Qi, W. J. Hoekstra, R. J. Schotzinger, J. D. York, F. P Guengerich and G. I. Lepesheva, *J. Biol. Chem.*, 2017, **292**, 6728–6743.

8 N. Liu, J. Tu, G. Dong, Y. Wang and C. Sheng, *J. Med. Chem.*, 2018, **61**, 5484–5511.

9 S. Emami, E. Ghobadi, S. Saednia and S. M. Hashemi, *Eur. J. Med. Chem.*, 2019, **170**, 173–194.

10 Z. Z. Yan, Z. B. Lv, D. Z. Zhao, M. B. Guo, Y. T. Wang, Z. Hou and C. Guo, *J. Mol. Struct.*, 2023, **1291**, 135997.

11 Z. Z. Yan, Q. Li, X. Y. Li, H. L. Wang, D. Z. Zhao, H. Yu, M. B. Guo, Y. T. Wang, X. Wang, H. Xu, Y. H. Mou, Z. Hou and C. Guo, *J. Med. Chem.*, 2024, **67**, 12601–12617.

12 H. Xu, C. Cao, X. Wang, M. B. Guo, Z. Z. Yan, R. An, R. Zhang, E. H. Dong, Y. H. Mou, Z. Hou and C. Guo, *Bioorg. Chem.*, 2021, **115**, 105182.

13 G. Han, N. Liu, C. Li, J. Tu, Z. Li and C. Q. Sheng, *J. Med. Chem.*, 2020, **63**, 5341–5359.

14 R. Pereira, R. O. Dos Santos Fontenelle, E. H. S. de Brito and S. M. de Morais, *J. Appl. Microbiol.*, 2021, **131**, 11–22.

15 X. Cui, L. Wang, Y. Lü and C. Yue, *J Infect Public Health*, 2022, **15**, 986–1000.

16 P. Marichal, L. Koymans, S. Willemsens, D. Bellens, P. Verhasselt, W. Luyten, M. Borgers, F. C. S. F. C. Odds and H. Vanden Bossche, *Microbiology*, 1999, **145**, 2701–2713.

17 Z. Li, J. Tu, G. Han, C. Sheng and N. Liu, *J. Med. Chem.*, 2021, **64**, 1116–1126.

18 Z. Z. Yan, Y. X. Huang, D. Z. Zhao, Z. Y. Li, X. Wang, M. B. Guo, Y. Wei, Y. T. Wang, Y. H. Mou, Z. Hou and C. Guo, *J. Med. Chem.*, 2023, **66**, 13247–13265.